

Processing reliant on granule cells is essential for motor learning but dispensable for social preference and numerous other cerebellar-dependent behaviors

Received: 9 March 2025

Accepted: 12 June 2025

Published online: 02 July 2025

 Check for updates

Joon-Hyuk Lee , Chong Guo, Shuting Wu, Aliya Norton, Soobin Seo, Zhiyi Yao  & Wade G. Regehr  

Mossy fiber inputs are transformed into cerebellar Purkinje cell (PC) outputs by granule cell (GC)-dependent processing. Cerebellar dysfunction leads to motor, learning, emotional, and social deficits that are usually attributed to altered PC firing arising from impaired processing of mossy fiber inputs, even though PCs also fire independently of GCs. To isolate their contributions to cerebellum-dependent behaviors, we either disrupt GC signaling while leaving PC firing intact, or disrupt PC signaling to eliminate the influence of PCs. Experiments were performed in mice of both sexes. We find that both GC and PC signaling are essential for eyeblink conditioning and vestibulo-ocular reflex (VOR) learning. Remarkably, disrupting PC signaling impairs VOR, anxiety, and social behavior, but abolishing GC signaling does not. This establishes that while GC signaling is critical for motor learning, it does not influence many behaviors including those associated with autism-spectrum disorder. It suggests that GC-independent behaviors can potentially be rescued by restoring altered firing in downstream regions.

The cerebellar cortex transforms mossy fiber (MF) firing patterns into PC outputs using a circuit consisting of the excitatory MF-GC-PC pathway and several types of intrinsic inhibitory interneurons. Abnormal PC signaling leads to deficits in motor performance¹, motor learning^{2,3}, and social deficits^{4–6} (symptoms associated with autism spectrum disorder, ASD), and various other behavioral abnormalities^{7–9}. PCs can influence these behaviors in two ways. First, PCs convey MF-GC-PC induced signals to the cerebellar nuclei (CbN). Second, PCs influence the CbN independently of GCs, either through their spontaneous firing (30–150 Hz¹ in the absence of synaptic inputs^{10,11}), which leads to ongoing inhibition of CbN neurons, or through climbing fiber activation (1–2 Hz), which induces complex spikes and a transient pause in firing^{12,13}. It is unclear whether PCs affect behaviors through GC-dependent or GC-independent mechanisms.

Disrupting PC signaling impairs both conditioned eyeblink learning and vestibular ocular reflex learning^{2,3}, but the importance of GCs in these behaviors is unclear. According to classic models, GCs are essential for motor learning¹⁴, and cerebellar learning is a consequence of associative plasticity at GC-to-PC synapses^{15–17}. However, a recent study found that impaired GC signaling delayed but did not prevent conditioned eyeblink learning, raising the possibility that eyeblink learning also occurs in the CbN independently of GCs¹⁸. The effects of disrupting GC signaling on VOR learning are unclear. While increased GC excitability does not significantly alter the changes in VOR gain during gain-down learning¹⁹, decreased GC signaling reduced the magnitude of VOR gain-down learning²⁰. However, GC signaling was not eliminated in these studies, and we previously found that only complete elimination of GC signaling can reveal the full extent of the

behavioral influence of GCs. For example, partial suppression of GC signaling did not alter gait and balance^{21–23}, but eliminating GC to PC synaptic transmission in GC-specific KO mice of Cav2.1, Cav2.2, and Cav2.3 did not alter the gross morphology of the cerebellum but severely impaired gait and balance¹. This suggests that it is necessary to eliminate GC signaling to determine the role of GCs in motor learning.

Reducing PC signaling also leads to social deficits and many other symptoms that are associated with ASD^{6,24}, but it is unclear if GC signaling is required for these behaviors. While early developmental disruption of granule cell neurogenesis causes gross structural abnormalities in the cerebellar cortex and leads to widespread behavioral deficits²⁵, it is not known if disrupting GC signaling at approximately 3 weeks (as for the Cre lines we use to target GCs^{26–28}) leads to social deficits. Moreover, it has been assumed that GCs are essential for social behaviors. For example, a recent study selectively deleted the ASD-related gene *SCN2A* from GCs and found that ocular reflexes were impaired similarly to those observed in ASD patients. The study speculated that disrupted GC signaling may also lead to social deficits^{29,30} (although this possibility was not tested). Accordingly, the role of GCs in social behavior remains controversial.

Here we determined whether various cerebellar-dependent behaviors rely on GC-dependent or GC-independent mechanisms by comparing the behavioral consequences of silencing PC or GC signaling. Based on the requirement that GC signaling must be eliminated to reveal the behavioral effects of GCs¹, we selectively eliminated Cav2.1, Cav2.2, and Cav2.3 rather than using chemogenetic or optogenetic approaches that provide superior temporal control but typically leave residual signaling intact^{31–34}. This approach also better approximates the long-term loss of cell signaling that occurs in cerebellar disorders³⁵. We find that disrupting signaling in either PCs or GCs abolishes conditioned eyeblink learning and VOR gain-down learning. In contrast, disrupting PC signaling impaired baseline behaviors such as VOR, anxiety-related behavior, and social behavior, whereas abolishing GC signaling did not. These findings establish that while GC-mediated cerebellar processing is essential for motor learning, many other cerebellum-dependent behaviors do not rely on GC signaling. We further find that disrupting PC signaling elevates the firing rates of CbN neurons, but disrupting GC signaling does not. This suggests that the subset of cerebellar behaviors that do not rely on GC-signaling, such as social behaviors and anxiety, could be rescued by simply restoring the altered firing rate in downstream regions without involving dynamic changes in PC signaling that arise from complex cerebellar processing mediated by GCs.

Results

The role of granule cell signaling in conditioned eyeblink learning

It is well established that disrupting PC signaling impairs conditioned eyeblink learning^{3,36} (Supplementary Fig. 1), but the effects of eliminating GC signaling are unclear. We therefore tested whether disrupting GC signaling influences motor learning in the conditioned eyeblink test. We used mice in which the calcium channels (Cav2.1, Cav2.2, and Cav2.3) that mediate synaptic transmission are conditionally eliminated using $\alpha 6$ -cre²⁷ and GABRA6-cre²⁸ to target GCs [GC ($\alpha 6$) TKO mice and GC (GABRA6) TKO mice, respectively]. In our previous study, we demonstrated that this triple calcium channel knockout method can effectively block granule cell signaling without causing gross morphological changes¹. Numerous previous studies have used these Cre lines to target GCs^{1,18–20,36–38}. The unconditioned stimulus (US) was an air puff that always caused the eye to close (Supplementary Fig. 2a), and the conditioned stimulation (CS) was illumination with a white LED. We measured the amplitude of eye closure by detecting the positions of the upper and lower eyelids (Fig. 1a, yellow and red dots) and the closed eyelid (Fig. 1a, orange dot) using deep learning. Experiments were conducted while mice walked

on a motorized treadmill at a modest speed (0.025 m/s) to promote rapid learning³⁹. Although GC TKO mice exhibit ataxia, they were able to walk on the treadmill under this condition, and this minimized secondary effects on learning that arise from differences in locomotion speed⁴⁰. Control mice showed progressively larger conditioned responses (CRs, i.e., eye closures) to the CS with training (Fig. 1a, top; Fig. 1b–d, Supplementary Movie 1). In contrast, GC ($\alpha 6$) TKO mice did not show CS responses, even after many days of training (Fig. 1a, bottom; Fig. 1b, second row), although they showed normal US responses (Fig. 1b, second row, Supplementary Fig. 2a). The CR amplitude (peak eyelid closures during 0.4–0.5 s after the start of LED illumination) of control mice gradually increased to an average of 77.6% on day 8, compared to 8.1% for GC ($\alpha 6$) TKO mice (Fig. 1c, top). The CR probability (percentage of CR responses above 50% amplitude) of control mice increased to an average of 72.5% on day 8, compared to 8% for GC ($\alpha 6$) TKO mice (Fig. 1c, bottom). Similar results were seen for GC (GABRA6) TKO mice (Fig. 1b, bottom row, Supplementary Fig. 2a, Supplementary Fig. 2b). The CR amplitude on day 9 was 85.2% for control mice compared to 1.5% for GC (GABRA6) TKO mice (Fig. 1d, top), and the CR probability was 83.3% and 0% for control mice and GC (GABRA6) TKO mice, respectively (Fig. 1d, bottom). Together, these results demonstrate that disrupting GC signaling abolishes motor learning in the conditioned eyeblink test.

The role of granule cell signaling in VOR learning

We also tested the extent to which GC signaling affects gain-down VOR learning. We performed VOR learning experiments while mice walked on a motorized treadmill at 0.025 m/s to standardize locomotor state and help keep mice awake and alert during prolonged training sessions. This approach was inspired by eyeblink conditioning experiments³⁹. In these experiments, VOR responses were measured before and after training sessions for four consecutive days (Fig. 2a). During test sessions, compensatory eye movements were monitored in head-fixed mice on the turntable in the dark during vestibular stimulation ($\pm 5^\circ$ turntable rotation at 0.5 Hz frequency) (Fig. 2b, left, Supplementary Movie 2). During training sessions, the same vestibular stimulation was accompanied by visual stimulation (vertical bars), moving left and right in phase with vestibular stimulation $\pm 5^\circ$, $\pm 7.5^\circ$, $\pm 10^\circ$, $\pm 10^\circ$ on days 1–4, respectively (Fig. 2b, right). There were six training sessions per day for four consecutive days. Control mice learned to reduce their compensatory eye movements and decrease their VOR gain, as shown by the progressive decrease in the angular velocity of compensatory eye movements (Fig. 2c, black). This learned response was apparent in all control mice tested but was not observed in GC ($\alpha 6$) TKO mice (Fig. 2d, orange) and GC (GABRA6) TKO mice (Fig. 2e, red). Similarly, the PC (PCP2) TKO mice, in which PC signaling is silenced by selectively eliminating Cav2.1, Cav2.2, and Cav2.3 from PCs¹, also failed to exhibit the learned response (Fig. 2f, blue).

The analysis of gain values from seven tests over each of the four days revealed that GC ($\alpha 6$) TKO mice had impaired motor learning throughout training days (Fig. 2g, orange) compared to control mice (Fig. 2g, black). We observed similarly impaired motor learning in GC (GABRA6) TKO (Fig. 2h) and PC (PCP2) TKO (Fig. 2i), which is also evident in a graph in which all mice are plotted collectively (Supplementary Fig. 3). These results establish that disrupting either GC signaling or PC signaling eliminates VOR learning.

The influence of silencing granule cell or Purkinje cell synapses on OKR, VOR, and VVOR

Thus far, we have shown that disrupting GC and PC signaling leads to similar deficits in gait, rotarod, and balance beam¹, and in motor learning for both eyeblink conditioning and VOR learning (Fig. 1, Supplementary Figs. 1, 2). We performed additional experiments to determine if other cerebellar-dependent behaviors are affected in a similar manner in GC TKO and PC TKO mice. We began by testing basic

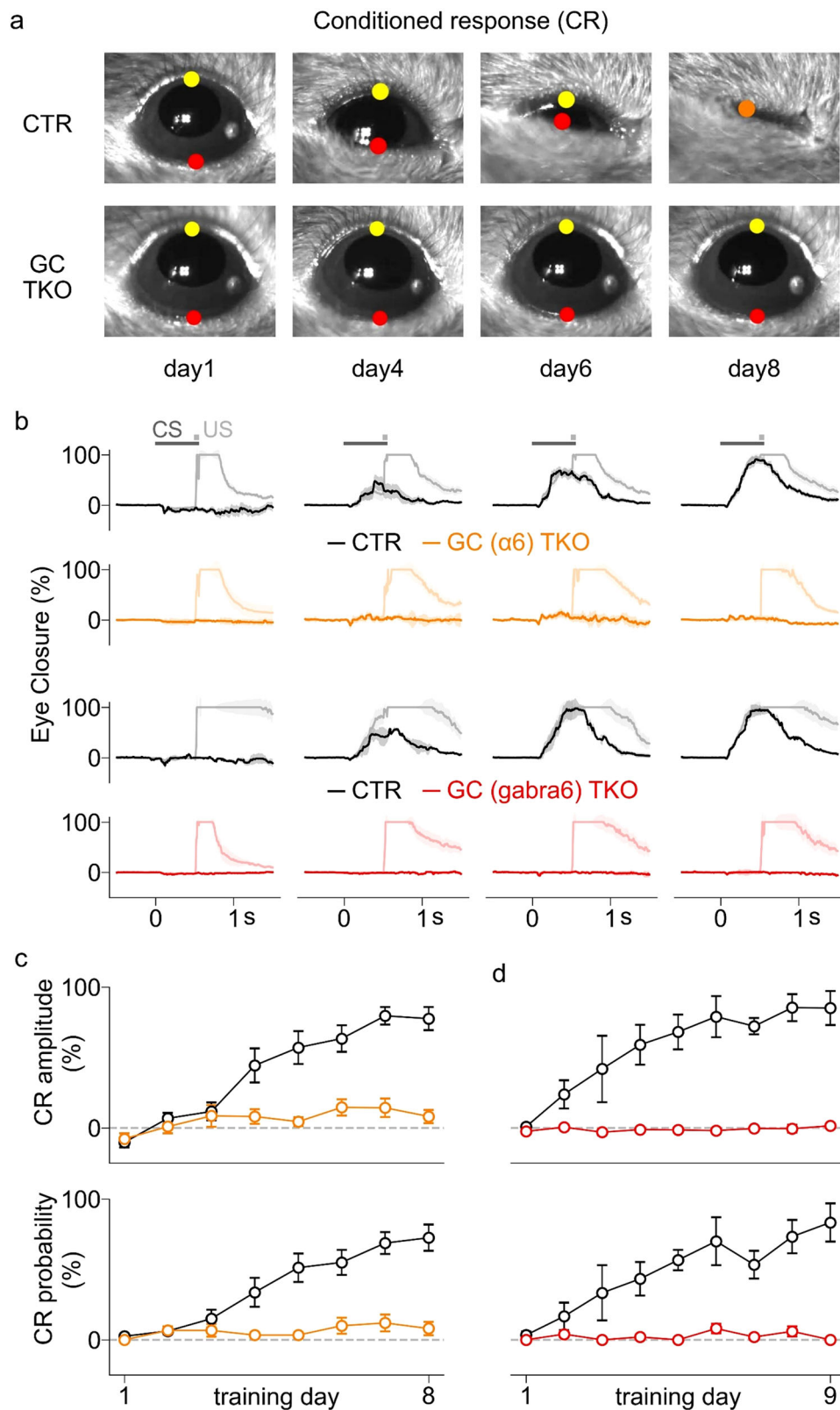
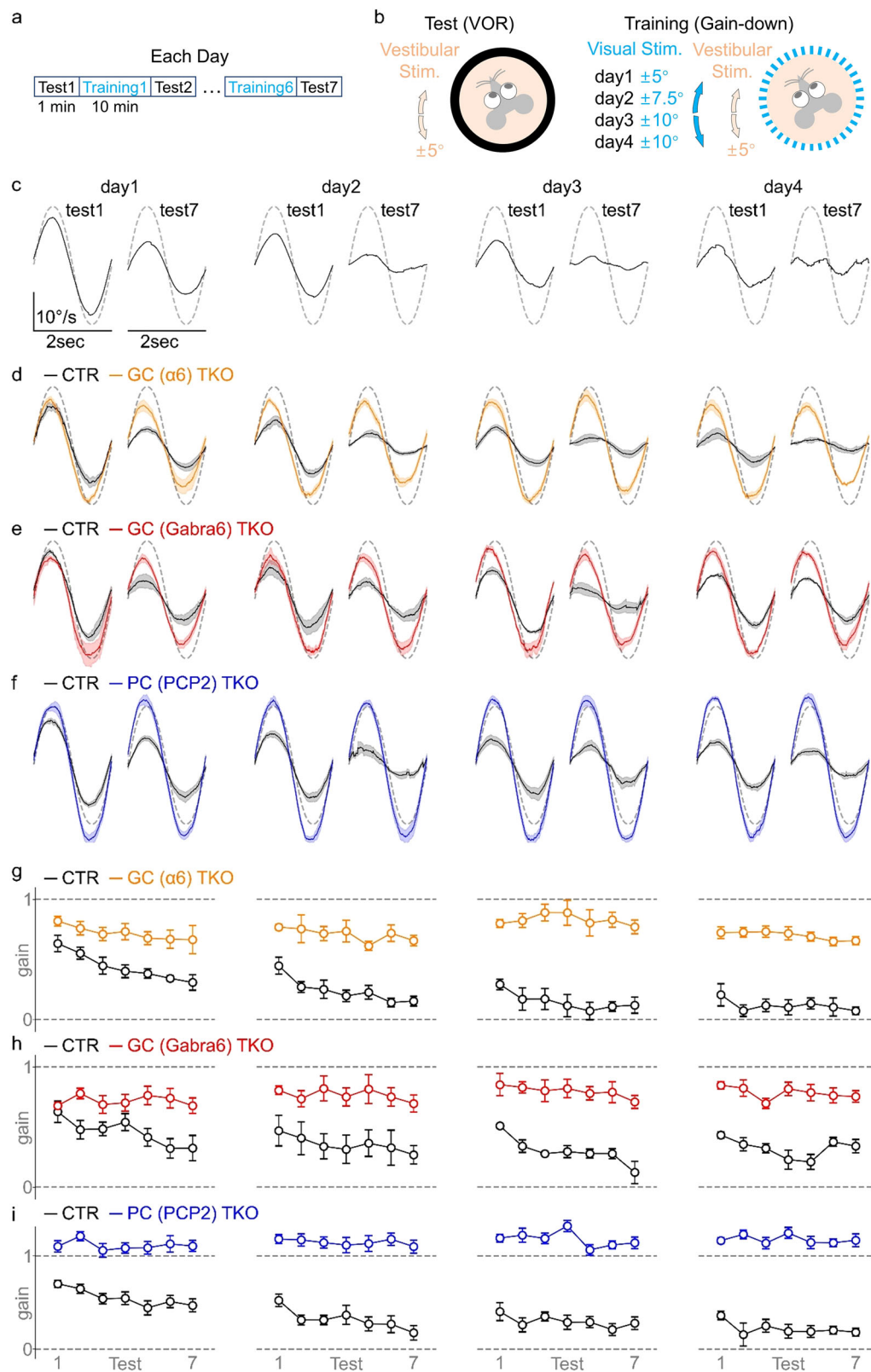


Fig. 1 | Granule cell signaling is essential for motor learning in the conditioned eye blink test. **a** Examples of conditioned responses of a control mouse (*top row*) and a GC ($\alpha 6$) TKO mouse (*bottom row*) on days 1, 4, 6, and 8. The yellow and red dots indicate the positions of upper and lower eyelid, and orange dot indicates the closed eyelid. The conditioned stimulus (CS, white LED) was presented at 0 s, and the unconditioned stimulus (US, air puff) was presented at 0.5 s. Also see Supplementary Movie 1. **b** Average eye closures are shown for GC ($\alpha 6$) TKO mice and

corresponding control mice (first two rows), and GC (GABRA6) TKO mice and corresponding control mice (third and fourth rows). CS-only trials (*dark*) and CS-US paired trials (*faint*) are plotted. The shaded area indicates SEM. **c** Average CR amplitude (*top*) and CR probability (*bottom*) are plotted for GC ($\alpha 6$) TKO and control mice. **d** As in (c) but for the GC (GABRA6) TKO group and control mice. The error bars indicate SEM. For statistics: **c**, **d** GC ($\alpha 6$) TKO and control: $n = 6$ and 8 mice, GC (GABRA6) TKO and control: $n = 5$ and 3 mice.



eye reflexes in the optokinetic reflex (OKR) test in which visual stimulation moved left and right $\pm 5^\circ$ without vestibular stimulation (Fig. 3a). As shown for a control mouse, we tested 0.2, 0.5, and 1 Hz stimulation (Fig. 3b) and compared the angular velocities of eye movements (Fig. 3b, left, black lines) and visual stimulation (Fig. 3b, left, dashed lines). These traces are normalized and replotted (Fig. 3b, middle), and the gain was determined for each frequency (Fig. 3b,

right). As established previously, OKR performance is superior for low frequency visual stimulation^{2,3,19,20}. Gain in the OKR assay was reduced in GC ($\alpha 6$) TKO mice for 0.5 and 1 Hz stimulation (Fig. 3c), in GC (GABRA6) TKO mice for 0.5 Hz stimulation (Fig. 3d), and in PC (PCP2) TKO mice for 0.5 and 1 Hz stimulation (Fig. 3e). These findings show that disrupting GC signaling and PC signaling similarly impairs OKR performance for 0.5 and 1 Hz stimulation.

Fig. 2 | Granule cell signaling is essential for motor learning in a VOR learning test. **a** A schematic summarizes the experimental protocol for each day in the 4-day VOR learning procedure. **b** A schematic describes the protocols for the gain-down training (left) and the test (right). During training, vertical bars moving left and right in front of the mice are presented in phase with the vestibular stimulus (i.e. turntable rotation). During testing, a vestibular stimulus is presented in the absence of visual stimulation, and the horizontal velocity of the pupil of left eye is monitored. **c** Example angular velocities of eye movements are shown for a control mouse (black traces) along with the velocity of vestibular stimulation (dashed lines). Note that these compensatory eye movements are in opposite phase with

vestibular stimulation, but they are inverted to aid in comparison to the visual stimulation. **d** Average eye movements are shown for GC ($\alpha 6$) TKO mice (colored) and control mice (black). The shaded areas indicate SEM. **e** Same as (**d**) but for GC (GABRA6) TKO mice. **f** Same as (**d**) but for PC (PCP2) TKO mice. **g** Changes in gain values measured in 7 tests each day for 4 days are shown for GC ($\alpha 6$) TKO mice (colored) and control mice (black). **h** Same as (**g**), but for GC (GABRA6) TKO mice. **i** Same as (**g**), but for PC (PCP2) TKO mice. The error bars indicate SEM. For statistics: **d–i**, GC ($\alpha 6$) TKO and control: $n = 6$ and 4 mice, GC (GABRA6) TKO and control: $n = 5$ and 3 mice, PC (PCP2) TKO and control: $n = 6$ and 5 mice.

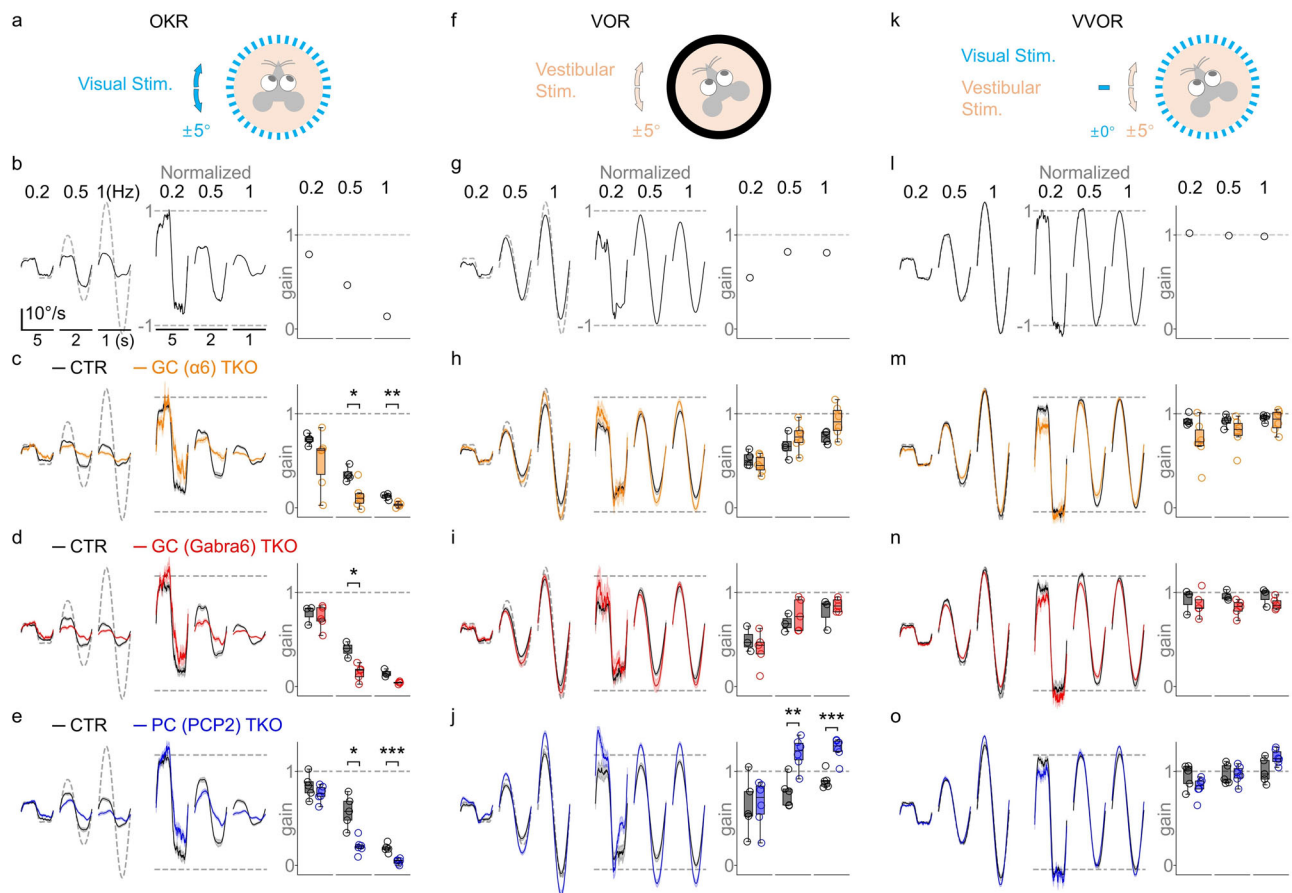


Fig. 3 | The effects of granule cell and Purkinje cell signaling on ocular reflexes. **a** A schematic is shown for an OKR test, in which visual stimulation (vertical bars moving left and right) is presented to a head-fixed mouse. **b** Example responses of a control mouse in the OKR test with visual stimulation at the indicated frequencies. Left, velocities of visual stimuli (gray dashed lines) and the corresponding pupil velocities (black lines) are shown. Middle, pupil velocities are replotted by normalizing to the peak velocities of visual stimulation. Right, gain values [(pupil velocity)/(peak velocity of visual stimulation)] are shown. **c–e** Average OKR responses are shown for GC ($\alpha 6$) TKO (**c**), GC (GABRA6) TKO (**d**), and PC (PCP2) TKO (**e**) mice. The solid lines and shaded areas (left and middle) indicate mean and SEM. Each circle (right) indicates a mouse. The definitions of box plot boundaries and components are detailed in the ‘Statistical Analysis’ section of the Methods. **f** A

schematic is shown for a VOR test, in which vestibular stimulation (turntable rotation) is presented in darkness. **g** Same as in (**b**) but for the VOR experiment with the dashed lines corresponding to vestibular stimulation. Pupil velocities in (**g–j**) are inverted for display purposes. **h–j** Same as in (**c–e**) but for the VOR test. **k** A schematic is shown for a VVOR test, in which vestibular stimulus is presented as in (**f**), but in combination with stationary visual stimulation. **l** Same as in (**g**) but for the VVOR test. Pupil velocities in (**l–o**) are inverted for display purposes. **m–o** Same as in (**c–e**) but for the VVOR test. For statistics: **c–e**, **h–j**, **m–o** GC ($\alpha 6$) TKO and control: $n = 6$ and 4 mice, GC (GABRA6) TKO and control: $n = 5$ and 3 mice, PC (PCP2) TKO and control: $n = 6$ and 5 mice. A two-way repeated measures ANOVA with Sidak’s multiple comparison test was used. * $p < 0.05$, ** $p < 0.01$, *** $p < 0.005$. Detailed statistical results are presented in Supplementary Table 1.

In the VOR test, vestibular stimulation was $\pm 5^\circ$ turntable rotation in the dark (Fig. 3f). As shown for a control mouse, we tested 0.2, 0.5, and 1 Hz vestibular stimulation (Fig. 3g) and compared the angular velocities of eye movements (Fig. 3g, left, black lines) with the angular velocity of vestibular stimulation (Fig. 3g, left, dashed lines). These traces are normalized and replotted (Fig. 3g, middle), and the gain was determined for each frequency (Fig. 3g, right). The properties of VOR were unchanged in GC ($\alpha 6$) TKO mice (Fig. 3h) and GC (GABRA6) TKO

mice (Fig. 3i). PC (PCP2) TKO mice exhibited an abnormal VOR response at 0.5 and 1 Hz stimulation in which the angular velocities of eye movements were larger than expected (Fig. 3j). Close inspection of the 0.2 Hz VOR responses also revealed a transient abnormal VOR response for 0.2 Hz stimulation in PC (PCP2) TKO mice (mean \pm sem, CTR, 0.74 ± 0.12 , TKO, 1.22 ± 0.11 ; t -test, $t(8.7) = 2.9$, $P = 0.017$), but not in GC ($\alpha 6$) TKO mice (CTR, 0.67 ± 0.05 , TKO, 0.82 ± 0.08 ; t -test, $t(7.5) = 1.5$, $P = 0.183$) or GC (GABRA6) TKO mice (CTR, 0.65 ± 0.03 ,

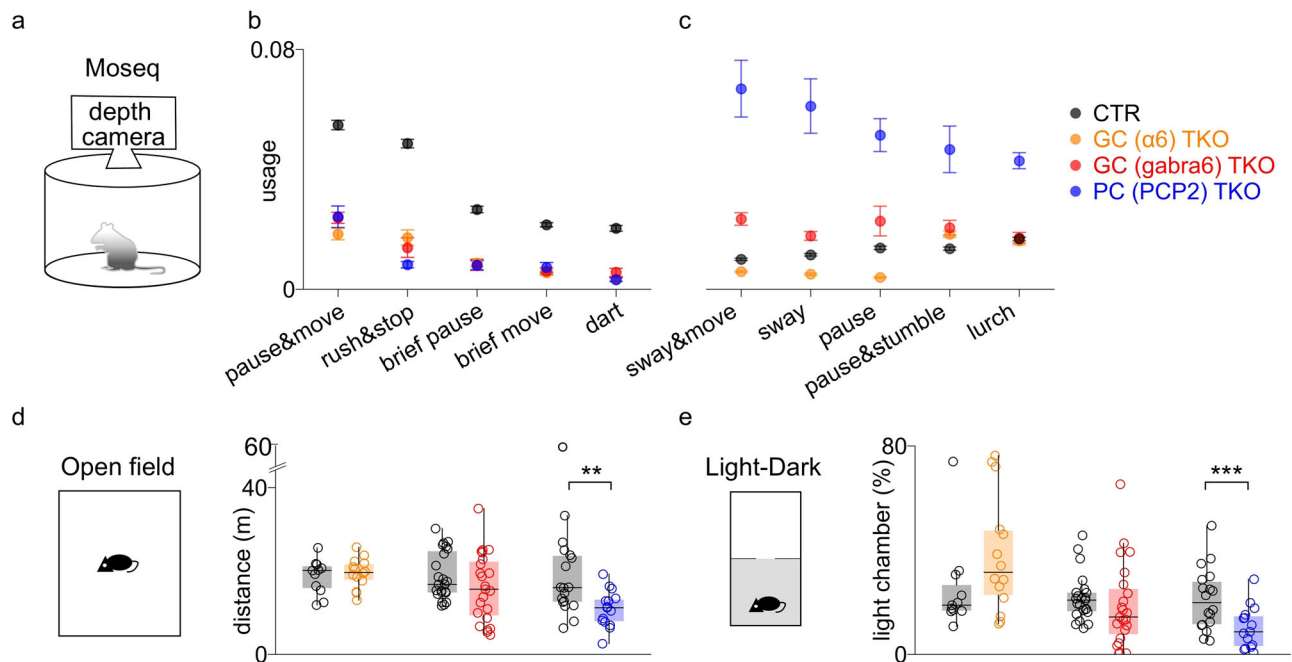


Fig. 4 | Disrupting granule cell and Purkinje cell signaling differentially influences specific spontaneous behaviors. **a** A schematic shows the MoSeq assay in which the 3D motion of mice is recorded by a depth camera. **b** MoSeq behavioral syllables that are observed less frequently in all TKO mice. **c** Syllables that are most frequently observed in PC (PCP2) TKO mice. The error bars indicate SEM. **d** A schematic of open field test and the distances traveled for control (black), GC (α6) TKO (orange), GC (GABRA6) TKO (red) and PC (PCP2) TKO (blue) mice are shown. Each symbol indicates a mouse. **e** A schematic of light-dark test and the time spent in the light chamber is shown for each group. The definitions of box plot

boundaries and components are detailed in the ‘Statistical Analysis’ section of the Methods. For statistics: **b, c** GC (α6) TKO, GC (GABRA6) TKO, PC (PCP2) TKO and control: $n = 9, 8, 6$, and 22 mice. **d, e** GC (α6) TKO and control: $n = 14$ and 11 mice, GC (GABRA6) TKO and control: $n = 23$ and 23 mice, PC (PCP2) TKO and control: $n = 15$ and 18 mice. A two-tailed t -test (**d** GC (α6) group; **e** PC (PCP2) group) or a two-tailed Mann-Whitney test (**d** GC (GABRA6) and PC (PCP2) group; **e** GC (α6) and PC (PCP2) group) was used. * $p < 0.05$, ** $p < 0.01$, *** $p < 0.005$. Detailed statistical results are presented in Supplementary Table 1.

TKO, 0.67 ± 0.15 ; Mann-Whitney test, $U = 6.0$, $P = 0.786$). These findings establish that disrupting GC signaling and PC signaling does not always influence behaviors in the same way.

The experimental protocol of the visually enhanced vestibulo-ocular reflex (VVOR) test is similar to the VOR test, with the exception that experiments are performed with stationary visual stimulation (Fig. 3k). The addition of visual stimulation greatly improves the performance of compensatory eye movements, and as shown for a control mouse, gain values at all frequencies were approximately one (Fig. 3l). VVOR performance was not impaired in GC (α6) TKO mice (Fig. 3m), GC (GABRA6) TKO mice (Fig. 3n) or PC (PCP2) TKO mice (Fig. 3o). These findings indicate that VVOR does not require the cerebellar cortex.

Influences of GCs and PCs on spontaneous behavior, locomotion, and anxiety

We then investigated how disrupting GC signaling and PC signaling affects spontaneous behavior by using the behavioral analysis platform Motion Sequencing (MoSeq) in which the movements of individual mice within a circular arena are monitored with a depth camera, and categorized as a series of distinct three-dimensional behavioral syllables that make up spontaneous behaviors (Fig. 4a)⁴¹. MoSeq has proven to be a useful tool to detect subtle variations in behavior in mouse models^{42,43}. We used MoSeq to characterize spontaneous behaviors in GC (α6) TKO mice, GC (GABRA6) TKO mice, PC (PCP2) TKO mice and their littermate controls to identify shared and distinct impairments in these mice. Behaviors of the three control groups were very similar, although minor differences were observed (Supplementary Fig. 4a). MoSeq revealed that some syllables were disrupted to a similar extent in both GC TKO and PC TKO mice (Fig. 4b, Supplementary Fig. 4c), as is the case for gait, balance beam and rotarod¹.

Other syllables were selectively altered in PC TKO mice (Fig. 4c, Supplementary Fig. 4d). The former syllables were all related to the initiation and cessation of locomotion (Supplementary Movie 3), whereas the latter were associated with swaying behaviors in a stationary state and with the initiation of motion (Supplementary Movie 3). Beyond these examples, GC TKO and PC TKO mice—as well as their respective control littermates—exhibited a range of both shared and divergent syllable usage patterns (Supplementary Fig. 4). Although the functional importance of these behavioral differences is unclear, this unbiased analysis of spontaneous behaviors revealed the important result that disrupting PC signaling and GC signaling differentially alters some spontaneous behaviors.

Subsequent experiments revealed that disrupting PC and GC signaling differentially influenced additional behaviors. In the open field test, locomotion was only reduced in PC (PCP2) TKO mice and was normal in GC (α6) TKO, GC (GABRA6) TKO mice (Fig. 4d). Further analysis of the speed in the open field test revealed that PC (PCP2) TKO mice spent more time in lower speeds (0–5 cm/s) and less time in high speed (20–100 cm/s), whereas GC TKO mice did not show differences compared to control mice (Supplementary Fig. 5b–d). The time spent in the center zone was unaltered in any TKO mouse line (Supplementary Fig. 5a). We also used a light-dark test to assess anxiety. Mice are naturally averse to bright light and tend to avoid a brightly illuminated chamber in favor of a dark chamber. The decreased time spent in the bright chamber is generally interpreted as reflecting an increase in anxiety-like behavior. We found that PC (PCP2) TKO mice spent less time in the illuminated chamber than littermate controls, but GC (α6) TKO and GC (GABRA6) TKO mice spent a comparable amount of time as littermate controls (Fig. 4e). One of the challenges of interpreting experiments in PC TKO and GC TKO mice is that their motor deficits could indirectly influence behaviors. However, the behaviors of PC

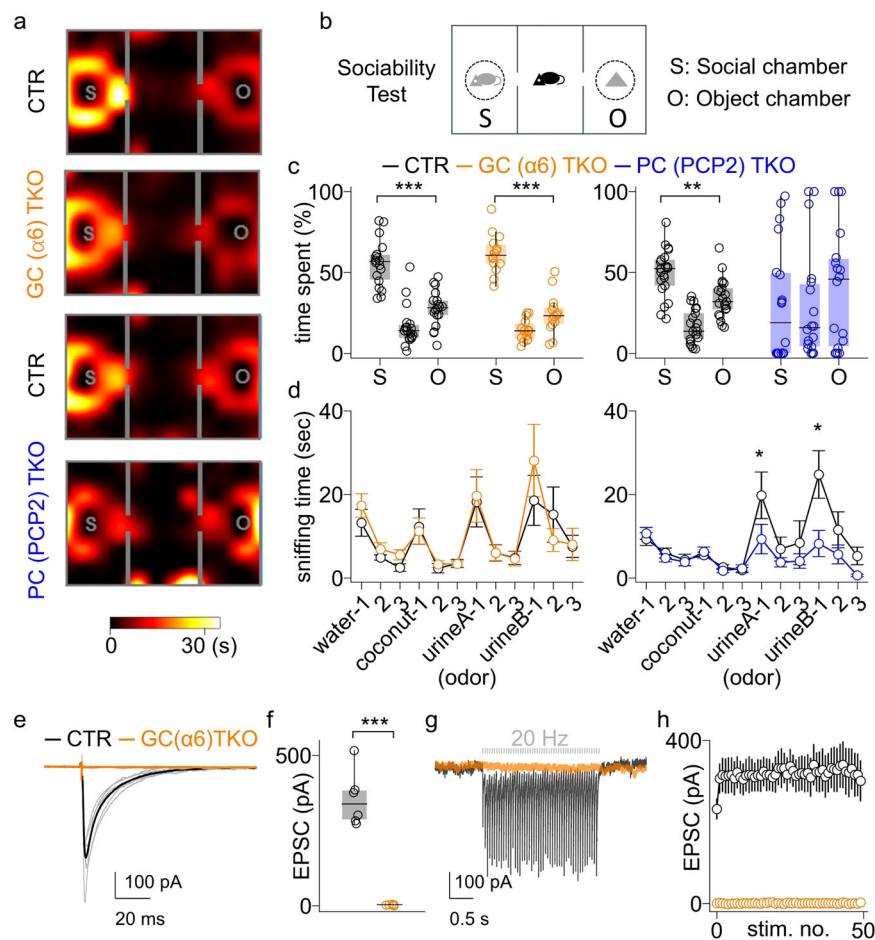


Fig. 5 | Granule cell signaling is dispensable for social behavior. **a** Heat maps show the time spent in the chambers during the sociability test. **b** A schematic of the sociability test. **c** The time spent in social chamber (S), middle chamber and object chamber (O) are shown for control (black), GC ($\alpha 6$) TKO (orange), and PC (PCP2) TKO (blue) mice. Mice did not show preferences for the social chamber before we introduced the stimuli (Supplementary Fig. 7a). Each circle indicates a mouse. The definitions of box plot boundaries and components are detailed in the ‘Statistical Analysis’ section of the Methods. **d** The sniffing time observed in the olfactory test is summarized. Neutral cues (water, coconut) and social cues (urine of same sex–urine A, opposite sex–urine B) were presented three times consecutively. The error bars indicate SEM. **e–h** GC-PC EPSCs were studied in brain slices from Crus I using whole-cell recordings. **e** GC-PC EPSCs of GC ($\alpha 6$) TKO (orange) and control (black) mice are shown. Responses from each cell (thin traces)

and average responses (bold traces) are shown. **f** Peak responses are summarized. Each circle is a cell. **g** Same as in (e), but for 20 Hz train stimulation. **h** Peak responses to 20 Hz stimulation are summarized. Error bars indicate SEM. For statistics: **a, c** GC ($\alpha 6$) TKO and control: $n = 14$ and 18 mice, PC (PCP2) TKO and control: $n = 18$ and 21 mice. A one-tailed paired t -test (GC ($\alpha 6$) TKO and control, PC (PCP2) TKO) or a one-tailed Wilcoxon signed-rank test (PC (PCP2) TKO) was used. **d** GC ($\alpha 6$) TKO and control: $n = 11$ and 10 mice, PC (PCP2) TKO and control: $n = 17$ and 17 mice. Statistical comparisons were performed on the responses to the first odor exposure using either a two-tailed t -test (GC ($\alpha 6$): urineA; PC (PCP2): water, coconut) or a two-tailed Mann-Whitney test (GC ($\alpha 6$): water, coconut and urineB; PC (PCP2): urineA and urineB). **f, h** GC ($\alpha 6$) TKO and control: $n = 5$ cells (1 mouse) and 6 cells (1 mouse). Two-tailed t -test was used. $^*p < 0.05$, $^{**}p < 0.01$, $^{***}p < 0.005$. Detailed statistical results are presented in Supplementary Table 1.

TKO mice and GC TKO mice in open field and light-dark assays differ, even though their gait and balance beam performance are impaired similarly¹. This suggests that the behavioral deficit in PC (PCP2) TKO mice in the light-dark test is not a simple consequence of motor deficits. Together, these findings reinforce the conclusion that disrupting PC signaling and GC signaling differentially affects various behaviors, including VOR, spontaneous behaviors, locomotion, and anxiety.

Granule cell signaling is not required for social behavior

We investigated how disrupting GC and PC signaling influences social behavior by using the three chamber assay, a widely used behavioral test for social behavior, in which the time spent near a social stimulus and an object are compared (Fig. 5b). Mice normally prefer to investigate a novel mouse rather than a novel object, as is the case for control mice in our experiments (Fig. 5a, c). Remarkably, in stark contrast to their severe deficits in motor functions¹ (Figs. 1, 2), GC ($\alpha 6$) TKO mice exhibited normal social preference and spent more time

near the social stimulus than the object stimulus, similar to control mice (Fig. 5a, c). Social preference was also intact in GC (GABRA6) TKO mice, although they also spent more time in the middle chamber (Supplementary Fig. 6a, b). Social preferences were intact for both male and female GC ($\alpha 6$) TKO and GC (GABRA6) TKO mice (Supplementary Fig. 7b). As anticipated, PC (PCP2) TKO mice did not show a preference to social stimulus (Fig. 5a, c). We also found that PC TKO mice that visited both the social and object chambers at least once failed to show any preference to the social stimulus (Supplementary Fig. 8), reinforcing the conclusion that their lack of social preference reflects a genuine behavioral deficit rather than reduced mobility. This illustrates the ability of the synaptic silencing approach we use to reveal social deficits. Whereas more minor disruptions of PC signaling seem to eliminate just social preference^{4–6}, we found that complete suppression of PC synapses also caused mice to spend extended periods of time immobile near the edge of the enclosure (Fig. 5a, bottom, middle chamber).

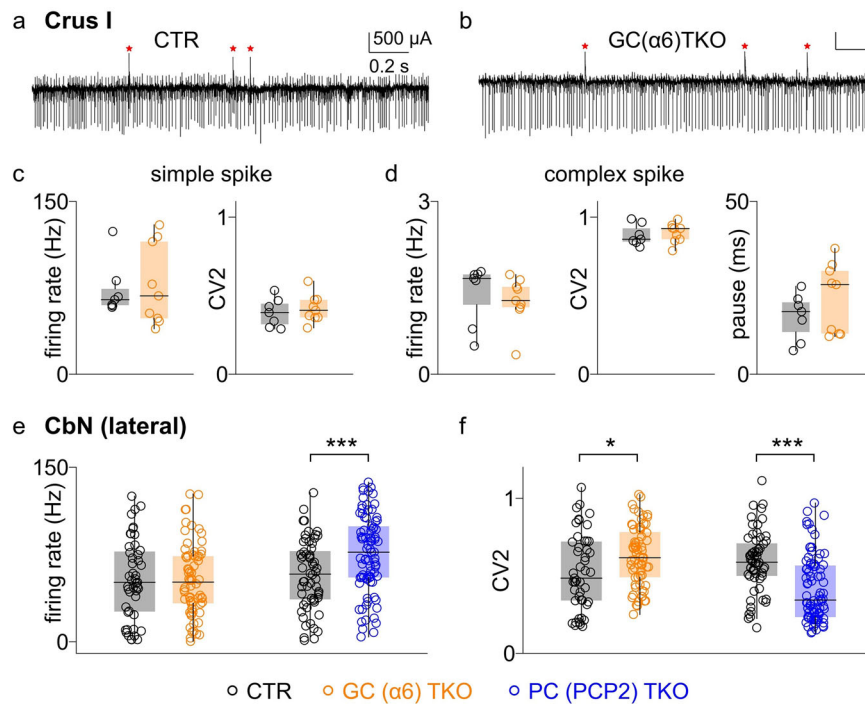


Fig. 6 | The effects of silencing GC synapses and PC synapses on in vivo firing properties. a–d PC firing in Crus I in vivo was examined in adult mice for GC (α6) TKO and control mice. **a** Simple spikes (downward spikes) and complex spikes (upward spikes marked as red asterisks) are apparent in a PC recording from a control mouse. **b** As in (**a**), but for GC (α6) TKO mouse. **c** Firing rates and variability (CV2) of control (black) and GC (α6) TKO (orange) mice are summarized for simple spikes. The definitions of box plot boundaries and components are detailed in the ‘Statistical Analysis’ section of the Methods. **d** PC complex spike firing rates, variability (CV2) and duration of the pause following the complex spike are shown

for control (black) and GC (α6) TKO (orange) mice. **e, f** Firing rates (**e**) and CV2 (**f**) of the lateral CbN neurons are summarized for control mice (black), GC (α6) TKO mice (orange) and PC (PCP2) TKO mice (blue). For statistics: **c, d** GC (α6) TKO and control: $n = 9$ cells (2 mice) and 7 cells (2 mice). **e, f** GC (α6) TKO and control: $n = 68$ cells (2 mice) and 47 cells (2 mice), PC (PCP2) TKO and control: $n = 60$ cells (2 mice) and 82 cells (2 mice). A two-tailed t -test (**d** GC (α6) group; **e** PC (PCP2) group) or a two-tailed Mann-Whitney test (**d** GC (GABRA6) and PC (PCP2) group; **e** GC (α6) and PC (PCP2) group) was used. * $p < 0.05$, ** $p < 0.01$, *** $p < 0.005$. Detailed statistical results are presented in Supplementary Table 1.

To further assess social preference in GC (α6) TKO mice, we performed an olfactory test, measuring sniffing time in response to both neutral and social odors. Genetic manipulations that target PCs have been shown to decrease the social preference and impair the detection of social odors^{6,44,45}. GC (α6) TKO mice showed normal sniffing responses to both neutral and social odors (Fig. 5d, left). PC (PCP2) TKO mice showed normal responses to neutral odors but significantly reduced responses to social odors (Fig. 5d, right), as is the case for other mouse models in which PCs are selectively manipulated and social preference is impaired^{4–6,45}.

One possible explanation for the normal social behavior observed in GC (α6) TKO mice was incomplete disruption of GC signaling in Crus I, which is the region of the cerebellar cortex involved in social behaviors^{4,5}. We previously showed that synaptic transmission was eliminated at GC-PC synapses in the vermis of GC (GABRA6) TKO mice¹, but diverse types of PCs and GCs are present in different regions⁴⁶. We therefore tested the possibility that the normal social behavior observed in GC (α6) TKO mice was due to incomplete disruption of GC signaling in Crus I. We used whole-cell electrophysiology to record GC-PC EPSCs in acute cerebellar slices containing Crus I from 8-week-old adult mice. We reliably evoked GC-EPSCs in Crus I of control mice, but no responses were observed in GC (α6) TKO mice (Fig. 5e, f). We also examined the possibility that prolonged high-frequency stimulation might reveal residual synaptic transmission. We stimulated GC inputs with trains of 50 stimuli and evoked sustained responses in control mice, but again did not observe any response in GC (α6) TKO mice (Fig. 5g, h). Synaptic transmission was also eliminated in Crus I of GC (GABRA6) TKO mice (Supplementary Fig. 6c–e). These results establish that intact social

behaviors in GC TKO mice do not reflect incomplete disruption of GC signaling.

Having confirmed that GC signaling in Crus I is eliminated in GC TKO mice, we examined whether disrupting GC signaling affects GC-independent PC activities, specifically PC spontaneous firing and complex spikes, in the Crus I region of GC (α6) TKO mice. To assess spontaneous firing, we measured simple spikes in a quiescent state. PCs fire two different types of spikes that are readily detected in extracellular recordings: simple spikes that are typical sodium-based action potentials that are present at high rates, and complex spikes that are present at 1–2 spikes/s and are evoked by neurons in the inferior olive that give rise to climbing fiber synapses (Fig. 6a). Both simple and complex spikes were also observed in GC (α6) TKO mice (Fig. 6b). The firing rate and variability of simple spikes (Fig. 6c) and complex spikes (Fig. 6d, left and middle) were not altered in GC (α6) TKO mice compared to littermate control mice. Complex spikes are followed by a pause in simple spike firing, and we found that the durations of such pauses following complex spikes were also unchanged (Fig. 6d, right). These findings indicate that disrupting GC signaling does not alter the spontaneous PC firing and complex spikes, and there are no compensatory changes in either PC firing or in the firing of inferior olivary neurons that give rise to climbing fibers.

Spontaneous firing in the deep cerebellar nuclei is regulated by PCs but not GCs

CbN neurons fire spontaneously^{47–50}, and their firing properties have been implicated in behavioral deficits. Alterations in CbN firing have been shown to impair social behavior^{4,51}, and altered firing variability has been observed in ataxic mouse models^{52–54}. Thus, it is possible that

disrupting PC synapses or GC synapses regulate spontaneous firing in the CbN in different ways, and this contributes to the differential behavioral effects in PC TKO mice and GC TKO mice. While it is anticipated that removing PC inhibition will increase spontaneous firing in CbN neurons, it is also possible that these neurons compensate for long-term changes in PC inhibition⁵⁵. We therefore assessed the firing properties of CbN neurons in PC TKO mice and GC TKO mice. Spike trains were analyzed during periods in which the mice were stationary. CbN neurons fire with a wide range of rates in control mice (Fig. 6e, gray), as shown previously for wildtype mice^{4,56–58}. In GC TKO mice, firing rates were not significantly different (Fig. 6e, orange), but there was a small but significant increase in the variability of firing (Fig. 6f, orange). In PC TKO mice, firing rates were significantly elevated (Fig. 6e, blue) and firing rate variability was reduced (Fig. 6f, blue). These findings suggest that eliminating either GC or PC signaling has distinct effects on ongoing firing in the CbN, and this could contribute to differential behavioral effects seen in PC TKO mice and GC TKO mice.

Discussion

A comparison of the behavioral effects of eliminating either GC or PC signaling revealed that the cerebellum regulates different behaviors through distinct GC-dependent and GC-independent mechanisms. GC and PC signaling were both essential for motor learning, OKR, and specific spontaneous behaviors, as well as for gait and balance, as shown previously¹. This establishes that these behaviors are mediated by GC-dependent mechanisms. In contrast, PC signaling was essential for normal VOR, specific spontaneous behaviors, locomotion, normal anxiety level, and social preference, while GC signaling was not required for these behaviors. This indicates that these behaviors depend on cerebellar cortex but rely on GC-independent mechanism. Eliminating PC signaling alters the firing rate of the CbN, whereas eliminating GC signaling does not. This suggests that deficits in GC-independent behaviors, such as social behavior, could potentially be rescued by simply restoring the altered firing rate in the CbN, without considering the complex processing in GCs.

The behavioral influence of PCs

Completely silencing PC synapses allowed us to attribute behavioral deficits in PC TKO mice to the lack of PC signaling¹, and the magnitude of the effects is expected to be larger than with partial suppression of PC signaling. This approach differs from most previous studies that examined the behavioral roles of PCs that were not designed to completely eliminate PC signaling. Numerous studies have determined the behavioral effects arising from selective PC targeting of genes implicated in movement disorders and autism spectrum disorder (for review, see Table 3 of ref. 59). These studies established the importance of PC signaling for movement and social disorders, but the observed behavioral effects could arise from decreased PC signaling or inappropriate PC firing.

PCs are known to be crucial to conditioned eyeblink learning^{3,36}, but there have been conflicting reports on whether PCs play an essential role in VOR learning. Some studies have shown that introducing inappropriate firing patterns in PCs impaired gain changes in gain-down learning, but did not eliminate the changes entirely^{2,19}, whereas another study reported that VOR learning was minimal³. Our results show that completely eliminating PC signaling abolished VOR gain-down learning (Fig. 2f, i), supporting the idea that PCs are essential for VOR learning. This learning deficit is unlikely to result from off-target Cre expression in retinal bipolar cells in the PCP2-cre line⁶⁰, because PC TKO mice exhibited normal responses in the VVOR test (Fig. 3o).

PC-TKO mice showed a large decrease in OKR gain (reduced to 35% of control; at 0.5 Hz CTR: 0.57, PC TKO: 0.20) (Fig. 3e), an increase

in VOR gain with a prominent overshoot (increased to 154% of control; at 0.5 Hz CTR: 0.79, PC TKO: 1.22, Fig. 3j) and unaltered VVOR gain (Fig. 3o). Our findings (Fig. 3e, o) are consistent with a previous study that suppressed PC firing by acute injection of the GABA_A-receptor agonist, muscimol, into the flocculus that reduced OKR gain from 0.84 to less than 0.5 (0.5 Hz stimulation) and minimally affected VVOR⁶¹. Thus, our genetic suppression of PC signaling has similar effects on OKR and VVOR as those arising from acute silencing of PCs in the monkey flocculus.

Social approach and social olfaction were strongly impaired in PC TKO mice, as in previous studies in which PCs were manipulated^{6,44,45,62,63}, or PCs in subregions perturbed^{4,5}. The social deficits we observed in PC TKO mice are unlikely to be secondary to motor impairments for several reasons. First, GC TKO mice exhibit motor deficits similar to PC TKO mice¹, yet still display normal social preference. Second, PC TKO mice that visited both the social and object chambers at least once did not exhibit social preference (Supplementary Fig. 8). Third, PC TKO mice exhibited a classic pattern of reduced investigation of social odors (Fig. 5d, right). PC TKO mice also spent prolonged periods immobile next to a wall. This behavior is not a simple consequence of impaired gait or balance, because GC ($\alpha 6$) mice are also ataxic but do not exhibit this behavior. Anxiety is also elevated by optogenetic activation of molecular layer interneurons in lobule VII of the vermis⁹, whereas inhibition of PCs in right Crus I led to social deficits^{4,5}.

Eliminating PC signaling increases the firing rate of CbN neurons

PCs fire at 10 to 100 spikes/s, their inputs are large (30 nS on average^{55,64}), and many PCs converge onto each CbN neuron, providing a noisy inhibitory tone that strongly suppresses CbN neuron firing⁶⁵. Removal of this inhibition can produce large and rapid increases in CbN neuron firing (~400%)³⁴ that are much larger than the increase in firing of CbN neurons (32%) that we observed in PC TKO mice. This indicates that CbN neurons compensate to a large extent for the lack of PC inhibition in PC TKO mice. Spike frequency adaptation of CbN neurons on the tens-of-seconds time scale⁵⁵ contributes to this adaptation, and additional mechanisms on longer time scales may also contribute.

GCs are essential for motor learning

We found that eliminating GC signaling prevents motor learning in the conditioned eyeblink test (Fig. 1) and prevents changes in gain down VOR learning (Fig. 2), which is consistent with classic models of cerebellar plasticity in which cerebellar learning arises from modifications of GC-PC synapses. To minimize the potential confound of motor impairments on learning performance^{39,40}, we performed eyeblink conditioning and VOR learning while mice walked on a motorized treadmill to standardize locomotor state and help keep mice awake and alert during prolonged training sessions. Importantly, wild-type mice eventually exhibit significant conditioned eyeblink responses regardless of treadmill speed³⁹, but GC TKO and PC TKO mice did not exhibit any conditioned responses even after 8 or 9 days of training, supporting the interpretation that in these mice, learning deficits arise from impaired cerebellar processing rather than differences in arousal or locomotion.

In a previous study in which inhibitory DREADDs were expressed in GCs, conditioned eyeblink learning was delayed but not eliminated, and it was concluded that slow onset learning was mediated by a mechanism within the CbN that did not involve GCs¹⁸. However, DREADDs can leave 30–50% of residual activity intact in vivo^{31–33} and it is highly unlikely that inhibitory DREADDs eliminate GC firing. As we do not see any learning in our experiments when we fully eliminate GC signaling (Fig. 2d, e, g, h), and see no indication of a mechanism that is independent of GC signaling, it is possible that reduced firing of GCs in

the presence of inhibitory DREADDs is still sufficient to produce eyeblink conditioning, albeit with a slower onset. Similarly, for VOR learning, GC-specific alterations of K-Cl cotransporters¹⁹ or deleting CaV2.1 calcium channels²⁰ led to less pronounced gain changes in gain-down learning than we observed, but both of these manipulations leave significant GC signaling intact. Meanwhile, one study found that reducing GC firing by deleting the *SCN2A* gene was sufficient to eliminate gain down learning in a 20 min training session²⁹, but it is not known how VOR learning is affected for more prolonged training (240 min over 4 days), as used in our study. PC-specific elimination of the AMPAR auxiliary subunit SHISA6 decreased GC-PC EPSCs by a factor of 3, but virtually eliminated VOR gain-down learning and conditioned eyeblink learning³. However, CF-PC synapses are also likely altered in adult SHISA6 mice, and these synapses play a crucial role in cerebellar-dependent plasticity and learning. Lastly, we show that although GC signaling is not required for VOR and VVOR, it is essential for OKR response (Fig. 3c, d, h, i, m, n), which was not apparent in studies in which GC signaling was suppressed but not eliminated^{19,20}. Together, these studies indicate that it is necessary to completely and selectively eliminate GC signaling to reveal the full extent of the influence of GCs on behavior.

GCs are not required for social preference

Surprisingly, social preference and responses to social odors were normal in GC TKO mice. What makes this even more remarkable is that GC TKO mice are ataxic, but this did not influence social preference. This was such an unexpected result that we checked for the possibility that the lack of effect might be due to remaining GC-PC signaling in Crus I region. However, we found that GC-PC synaptic transmission was eliminated in GC TKO mice, indicating that intact responses to social odors and the normal social preferences could not be explained by residual synaptic transmission (Fig. 5e–h).

This result has important implications for the study of *SCN2A*, which is a major risk factor for ASD that is associated with heightened responses to sensory stimuli. The presence of *Scn2a* (Nav 1.2 encoding gene) in GCs, combined with the observation that heterozygous expression of Nav 1.2 in GCs leads to hypersensitive VOR²⁹, raised the possibility that reduced expression of Nav 1.2 in GCs could be the cause of ASD in *SCN2A* patients. Our results suggest that decreasing GC signaling alone is insufficient to produce social deficits, and that it is important to directly examine social behaviors in mice with selective heterozygous loss of Nav 1.2 in GCs.

Although GCs are not required for social preference, that does not mean that GCs in Crus I do not have functional roles. Just as GCs are not important regulators of baseline VOR but they are essential for gain-down VOR learning, it is likely that GCs allow the cerebellum to learn new social responses.

Different behavioral effects of eliminating and increasing GC signaling

It is worth noting that eliminating GC signaling influences behaviors so differently than increasing GC excitability. We previously selectively eliminated the GABA_A δ subunit from GCs (Cb δ KO mice) to attenuate tonic GC inhibition. This, in turn, made GCs much more excitable. Whereas eliminating GC signaling had profound effects on most motor behaviors¹ and motor learning (Figs. 1, 2), in Cb δ KO mice motor performance and motor learning were normal. We also found that anxiety was unaffected in GC TKO mice but was elevated in Cb δ KO mice. Lastly, there are no social deficits in GC TKO mice, whereas social behaviors are altered in females in Cb δ KO mice³⁷. The behavioral differences that arise from completely silencing GC synapses or increasing GC excitability highlight the differences in insights that can be obtained by increasing or decreasing the influence of a particular cell type.

Comparison of the behavioral influences of GCs and PCs

A comparison of the effects of eliminating PC and GC signaling establishes that most cerebellum-dependent behaviors tested are cerebellar cortex-dependent and, surprisingly, a significant subset of these behaviors do not require GC-dependent processing (Table 1). Performance on balance beam, rotarod, gait, OKR, and specific spontaneous behaviors (Fig. 4b), as well as VOR learning and conditioned eyeblink, are all impaired similarly in GC TKO mice and PC TKO mice, indicating that these behaviors rely on GC-dependent mechanism, and are cerebellar cortex-dependent. In contrast, GC TKO mice did not exhibit a number of behavioral deficits that were observed in PC TKO mice: (1) there was no prominent overshoot in VOR (Fig. 3h, i, j), (2) specific spontaneous behaviors were unaffected (Fig. 4c), (3) the distance traveled was not impaired (Fig. 4d) and the slow and rapid components of movement was intact (Supplementary Fig. 5b–d), (4) anxiety levels did not increase (Fig. 4e), and (5) social preference and responses to social odors were normal (Fig. 5a–d). This indicates that these behaviors are cerebellar cortex-dependent but do not require GC-dependent processing. In addition, the consistent results observed in GC ($\alpha 6$) TKO and GC (GABRA6) TKO mice, along with the shared motor deficits in balance, rotarod performance, and gait reported in our previous study¹, help to alleviate concerns about off-target Cre expression associated with the different Cre lines^{27,28} used to generate these two GC TKO models. However, minor behavioral differences between GC ($\alpha 6$) TKO and GC (GABRA6) TKO mice in the MoSeq analysis (Supplementary Fig. 4b) suggest that the Cre lines have small differences.

It is well established that particular regions of the cerebellar cortex influence specific behaviors^{5,61,66,67}, and it was generally assumed that the same basic circuit is repeated throughout the cerebellar cortex and that different regions regulate different behaviors using the same basic circuit that adjusts the weights of GC-PC synapses to transform a pattern of mossy fiber inputs into a pattern of PC outputs. The stark contrast between severely impaired motor learning (Fig. 2g) and normal social behavior (Fig. 5c, left) observed in GC-TKO mice clearly demonstrates that not all cerebellum-dependent behaviors are mediated by the same conventional cerebellar processing that relies on GC-PC synapses.

These findings have important implications for rescuing deficits that arise from cerebellar dysfunction. Behaviors that rely on GC signaling involve complex and dynamic PC firing mediated by GC signaling, making the correction of these behaviors is expected to be exceedingly difficult. In contrast, our results suggest that VOR overshoot, elevated anxiety, and deficits in social preference do not involve GC-dependent processing. The most likely explanation is that the elimination of spontaneous PC firing in PC TKO mice leads to these deficits, as previous studies have shown that a decreased spontaneous PC firing rate is linked to social deficit^{4,5}. We have shown that the lack of spontaneous PC firing disinhibits neurons in the CbN, which, in turn, is expected to increase firing in downstream regions. This raises the possibility that rescuing such behaviors is a matter of suppressing the firing of neurons in downstream regions. This is exactly what was previously observed in an autism mouse model, where mice exhibiting social deficits due to decreased PC firing in Crus I of the cerebellar cortex showed elevated firing in the contralateral prefrontal cortex, and suppressing firing in the prefrontal cortex rescued social behaviors^{4,5,45}. These studies suggested that ASD could be treated by elevating PC activity or by suppressing the activity of appropriate downstream regions. Our results suggest that such a therapeutic strategy was successful for social deficits, because they are not reliant on granule-cell dependent processing. Our results also suggest that a similar strategy could also be effective in treating the subset of cerebellar dependent deficits that do not rely on GC-dependent processing, such as VOR overshoot and elevated anxiety.

Table 1 | Behavioral effects of silencing the output of the cerebellar cortex (PC TKO) or the input layer of the cerebellar cortex (GC TKO)

	PC-TKO	GC-TKO	
Conditioned eyeblink			Fig. 1 Supplementary Fig. 1
VOR learning			Fig. 2
Balance beam			Lee et al. 2023
Rotarod			Lee et al. 2023
Gait			Lee et al. 2023
OKR			Fig. 3a-e
VOR			Fig. 3f-j
VVOR			Fig. 3k-o
MoSeq (spontaneous behaviors)			Fig. 4b-c
Open field (locomotion)			Fig. 4d
Light-dark test (anxiety)			Fig. 4e
Three chamber test (social preference)			Fig. 5a-c
Olfaction test (social odors)			Fig. 5d

Dark gray indicates an impairment in behavior, and light gray indicates that the behavior is unaffected. The left column indicates the names of the behavioral assays used, and the italicized text in parentheses represents the specific traits measured in each assay. Some of the results have been extracted from our previous publication¹.

Methods

Mice

Animal procedures were carried out in accordance with the NIH and Animal Care and Use Committee (IACUC) guidelines, and protocols approved by the Harvard Medical Area Standing Committee on Animals. Male and female mice were used for experiments. Mice were kept on a mixed background (129 Sv/SvJ and B6/C57). Mice were housed under standard conditions in groups of 2–5 animals on a 12 h light-dark cycle at an ambient temperature of 22 °C and ambient relative humidity of 50%, with food and water available *ad libitum*.

We generated GC (α6) TKO, GC (GABRA6) TKO, and PC (PCP2) TKO mice as we described previously¹. Briefly, we utilized the previously described mouse line that had floxed alleles for the conditional ablation of CaV2.1, CaV2.2, and CaV2.3. (*floxed* CaV2s line)²⁶. This mouse line was crossed with α6-cre line (RRID:MMRRC_000196-UCD) for GC (α6) TKO, Gabra6-cre line (RRID:MMRRC_000213-UCD) for GC (GABRA6) TKO, and Pcp2-cre line (Jackson laboratory, Strain# 010536) for PC (PCP2) TKO, to produce the mice with the genotype Cre(+); CaV2.1(*flox/flox*), CaV2.2(*flox/flox*), CaV2.3(*flox/flox*). The littermate mice with the genotype Cre(-); CaV2.1(*flox/flox*), CaV2.2(*flox/flox*), CaV2.3(*flox/flox*) were used as control mice.

Behavioral testing

All motor behavior testing was conducted on adult male and female mice, with the experimenter blinded to the genotype. For conditioned eyeblink tests, the 10–11 week old mice were used. For VOR learning and OKR/VOR/VVOR experiments, 9–10 week old mice were used. For MoSeq experiment, 11–15 week old mice were used. For open field test, light-dark test, and three chamber test, 8–13 week old mice were used. For olfaction test, 7–34 week old mice were used. Before behavioral

testing, mice were handled by experimenter for 15 mins for two days. On the test day, mice were transferred to the behavior room and allowed to acclimate for at least 30 min. Apparatuses used for behavioral testing were cleaned with 70% ethanol between experiments. Two types of learning experiments—VOR learning and eyeblink conditioning—were conducted sequentially on the same mice. Eyeblink training began three days after the completion of VOR learning. In a separate cohort of mice, behavioral tests were performed in the following order: open field test, light-dark test, and three chamber test, with intervals of 2 h and 1 day between tests, respectively. Some of the mice used for the olfaction test and MoSeq assay had previously participated in the three chamber test, while others had not. For those that had, the subsequent experiments were conducted at least two weeks later. The interval between the olfaction test and the MoSeq assay was at least one week.

Conditioned eye blink test

Before the experiment, mice were implanted with a head bracket and allowed to recover for at least five days post-surgery. Then, one day of habituation was performed before the first day of eyeblink training to accustom the animals to the apparatus. During the habituation, the mouse was head-fixed for 20 min atop a motorized treadmill with six inches in diameter, rotating at 2.5 cm/sec. During the training, a white LED flash to the left eye with 550 ms duration was used as the conditioned stimulus (CS), which was co-terminated with the unconditioned stimulus (US) (periorbital air puff 2 psi for 5 ms) to the right eye. A hundred CS-US paired trials and ten CS-only trials were randomly assigned and tested with a mouse per day. The intervals between the trials were randomized between 4 and 12 s. The training lasted for 8–9 days. During the trials, the right eye was recorded by a high-speed IR camera (Mako U-029B; Allied Vision, Exton, PA) and a macro lens (1/2

inch, 4–12 mm F/1.2, Tamron, Commack, NY) at 280 fps. To detect eye blink events, the positions of the upper and lower lids in the recorded videos were detected by an open-source deep neural network, DeepLabCut⁶⁸. Then, the vertical distance between the upper and lower lids was analyzed. The pneumatic and electronics necessary for the control of the air puff were based on the design of Openspritzer⁶⁹. The CR amplitude was defined as the average eye closure value measured between 0.4 and 0.5 s after the LED was turned on. The CR probability was defined as the percentage of events where the CR amplitude exceeds 50%. Analyses were performed using custom MATLAB and Python code.

OKR/VVOR/VOR and VOR training

Before the experiment, mice were implanted with a head bracket and allowed to recover for at least five days post-surgery. During the test, the mice were head-fixed on the treadmill (speed, 2.5 cm/sec) with their left eye at the center of a custom-made VOR apparatus. The apparatus was fully enclosed for light control and includes a motorized turntable powered by a servo motor (CPM-MCVC-2341S-RLS; Teknic, inc.), delivering horizontal vestibular stimuli. The cylindrical paper screen surrounding the mouse with a 25 cm distance from the left eye was used to present the visual stimuli generated by Laser Screen Beam Projector (MP-CL1A, 1920×720; Sony, Inc.). The visual stimuli were the vertical bars spaced by 7 degrees with 3-degree widths, and moved back-and-forth horizontally by $\pm 5^\circ$. The left eye is recorded by a high-speed IR camera (Mako U-029B; Allied Vision, Exton, PA) at 200 fps with 640×480 pixel resolution. A multifunction I/O device (PCIe-6321; NATIONAL INSTRUMENTS CORP.) was used to monitor the table rotation and to command the servo motor and the camera. The visual stimuli, I/O device, and camera were controlled by a custom-made GUI MATLAB application. An infrared LED fixed to the top of the camera was used to make corneal reflection on the left eye. The infrared LED to illuminate the left eye was positioned below the camera. One day before the experiment, the mice were habituated on the apparatus for 20 min. During the experiments, pilocarpine (4% ophthalmic drops; Patterson Vet Supply, Inc.) was applied to the left eye to limit pupil dilatation to accurately track the eye movement in darkness.

Right before the eye recording, we took pictures of the pupil of each mouse while moving the camera back-and-forth around the vertical axis of the turntable with a known angle ($\pm 10^\circ$) to calculate the radius of pupil rotation (R_p) that was used to convert the pixel position to angular position of the eye (Stahl et al., 2000). R_p values were measured at three different pupil diameters by calculating $R_p = \Delta / \sin(20^\circ)$, where Δ is the pixel distance between the centers of the pupils, determined by their relative position to the corneal reflection in images taken at $\pm 10^\circ$. Then, the R_p regression line was made to estimate the R_p values with various pupil diameters. The angular eye movement was calculated by the following formula: angular eye movement between t_1 and $t_2 = \arcsin[(P_{t_1} - CRF_{t_1}) - (P_{t_2} - CRF_{t_2})/R_p]$ where P is the pupil center position, CRF is the position of corneal reflection, and R_p is the value estimated by R_p regression line for the corresponding pupil diameter.

In optokinetic reflex (OKR) test, the left eye was recorded while the different frequencies of visual stimuli (0.2, 0.5, and 1 Hz) with a fixed $\pm 5^\circ$ amplitude were presented while the turntable was fixed. In vestibulo-ocular reflex (VOR) test, the left eye was recorded in complete darkness while the turntable was rotating back-and-forth with different frequencies (0.2, 0.5 and 1 Hz) with a fixed $\pm 5^\circ$ amplitude. The visually guided VOR (VVOR) test was the same as the VOR test, except the fixed visual stimuli were presented. In VOR training, the visual stimuli and the turntable were rotated in phase (at the same amplitude, $\pm 5^\circ$) on Day 1. On Day 2–4, the visual stimuli were rotated in phase to the turntable rotation but with greater amplitudes (Day2, $\pm 7.5^\circ$; Day3, $\pm 10^\circ$; Day4, $\pm 10^\circ$), while the amplitude of the turntable remained $\pm 5^\circ$. On each training day, 6 × 10 min VOR trainings were performed, and 7 VOR tests were performed before, between, and

after the trainings, to probe the effect of the trainings. In VOR training, the frequencies of the visual stimuli and the turntable were both 0.5 Hz. In VOR tests, the frequency of the turntable is 0.5 Hz.

In the acquired video, the pupil center was detected using an open-source deep neural network, DeepLabCut⁶⁸. After the pixel velocity of the pupil center was converted to angular velocity, a low-pass filter set at twice the stimulation frequency was applied. Data exceeding $40^\circ/\text{sec}$ was removed from further analysis to exclude saccadic eye movements, except for VOR response analysis, where a threshold of $60^\circ/\text{sec}$ was applied. This was because PC-TKO mice exhibited non-saccadic VOR responses exceeding $40^\circ/\text{sec}$. Gain values were calculated as the ratio of the amplitude of angular eye velocity to the angular velocity of either the visual stimulus or the turntable velocity. Analyses were performed using custom MATLAB and Python code.

Motion sequencing

Motion Sequencing (MoSeq)-based behavioral analysis was performed as in the previous studies^{37,41,42}. In brief, MoSeq uses unsupervised machine learning techniques to identify the number and content of behavioral syllables out of which mice compose their behavior; identifying these syllables allows each video frame of a mouse behavioral experiment to be assigned a label identifying which syllable is being expressed at any moment in time. Behavioral phenotypes that distinguish wild-type and mutant mice can be identified by comparing differences in how often individual syllables are used in each experiment. Here, individual mice are imaged for three 30-minute-long sessions using a Kinect2 depth sensor while behaving in a circular open field. These 3D imaging data are submitted to the MoSeq pipeline⁴¹.

Open field test

During this test, an animal was placed in uncovered rectangular behavior arena (30.3 cm × 45.7 cm, 30.5 cm high) and allowed to explore for 10 min, under dim (40 lux) lighting. The position of the mouse was tracked using custom MATLAB scripts. The travel distance and the time spent in the center zone, corresponds to the four central areas when the bottom surface is evenly divided into 16 sections, were calculated.

Light-Dark test

The light-dark chamber (40 cm × 20 cm) consisted of a light chamber (>600 lux) and a dark chamber (<10 lux). A door between two chambers allowed the mice to freely explore the two chambers. At the beginning of the experiment, the mouse was placed in the dark chamber and allowed to freely navigate both chambers for 10 min with videotaping. The position of the mouse was tracked using custom MATLAB scripts. Then, the ratio of time spent in the light chamber over the dark chamber was analyzed.

Three chamber assay

The arena consisted of a clear rectangular Plexiglas box (40.5 cm wide, 60 cm long, 22 cm high) without a top cover and was divided into three equally sized compartments by two transparent walls. Each wall contains a $10.2 \text{ cm} \times 5.4 \text{ cm}$ rectangular door to allow the mice to navigate between the compartments. First, mice were pre-exposed to the middle chamber for 5 min, with the doors to the adjacent chambers closed, to maximize the exploration time in the side chambers during the test. Then, during a 10 min baseline session, the doors are opened, and mice were allowed to freely navigate all three chambers for 10 min. After that, the doors were closed again while the animal remains in the middle chamber. Then, a wire cup (10 cm in diameter) containing a social stimulus (juvenile mouse aged 15–30 days of the same sex) was placed in either the right or left chamber. Also, a wire cup containing a novel object (mouse-sized plastic toy, Schleich GmbH, Germany) was placed in the opposite chamber. The sides of social and object stimuli were randomly selected to control for preference to either side of the

arena. After the stimulus placements, the doors were opened, and the animal was observed for another 10 min. The time spent in the social chamber and object chamber were analyzed offline using a custom-made MATLAB code.

Olfaction test

The experiments were performed in the dark environment (<10 lux). Mice were placed in a transparent chamber (18 cm wide, 32 cm long, 13 cm high) with 2–3 mm bedding and habituated with a cotton-tipped applicator without odor for 30 min. The cotton tip was placed 2 cm above the bottom in the middle of the chamber. Then, the cotton tip with 10 μ L of odor was presented three times for 2 min each. For each 2 min recording, the cotton tip was replaced with a new cotton tip with the same odor. During the presentation, the mice were videotaped by IR camera (EPL IR USB camera, 30 Hz frame rate). In this way, water, coconut, urine A (same sex), urine B (opposite sex) were presented. The coconut odor was 10 times diluted from the original liquid (McCormick, Inc.). The urine samples were collected from unfamiliar, sex-matched adult mice aged over 7 weeks. In the recorded videos, the odor responses were manually counted by the experimenter blind to the genotype. The odor responses were defined by the sniffing behavior when mouse's nose was facing the cotton tip and the distance to the cotton tip was less than 3 cm.

In vivo recording

To prepare for in vivo recordings, mice (9–10 week old) were anesthetized with isoflurane (4–5% induction, 1–3% maintenance) and implanted with a custom-made titanium head bracket. A small craniotomy (0.5–1 mm diameter) was drilled over the Crus I (2.4 mm from the midline, –6.0 mm posterior to the bregma) to enable recordings from both Crus I and CbN. The cranium above the anterior cerebellum remained exposed and was covered with Kwik-Sil, a silicone polymer, at the end of the surgery. Mice were allowed to recover from surgery for at least five days. For acclimation, mice were head-restrained on a free-moving cylindrical treadmill for at least 30 min the day before recording. On the day of recording, the silicone polymer covering the cranial window was removed, and a silicon probe (64 channel probes, Cambridge NeuroTech) dipped in Di-I (Vybrant Multicolour Cell Labelling Kit, ThermoFisher) was inserted into the brain at an angle of approximately 20 degrees from perpendicular. The probe passed through the Crus I region and reached the lateral CbN. In vivo recordings were performed while the mouse was in a quiescent state. Data were sampled at 20 kHz using an RHD2000 recording system (Intan Technologies) and filtered between 0.1 and 8 kHz. PCs were distinguished by the presence of complex spikes. When recordings were complete, mice were perfused with PBS and 4% PFA. 100 μ m coronal slices are made from the brain tissue to confirm recording location in Crus I and CbN. Single units were sorted using open-source modules, Kilosort⁷⁰, SpikeInterface⁷¹, and Phy2 (<https://github.com/cortex-lab/phy>). Analyses were performed using custom Python code.

Slice preparation for electrophysiology

Male mice of 8 weeks old were used for in-vitro physiology experiments. Animals were anesthetized with ketamine/xylazine/acepromazine and transcardially perfused with warm choline-ACSF solution containing in mM: 110 Choline Cl, 2.5 KCl, 1.25 NaH₂PO₄, 25 NaHCO₃, 25 glucose, 0.5 CaCl₂, 7 MgCl₂, 3.1 Na-Pyruvate, 11.6 Na-Ascorbate, 0.005 NBQX, and 0.0025 (R)-CPP, oxygenated with 95% O₂/5% CO₂. To prepare sagittal slices of the cerebellum, the hindbrain was first removed. A cut was made down the cerebellar midline, and the two halves of the cerebellum were glued with the medial face down to the slicing chamber. 150–200 μ m thick sagittal slices were cut with a Leica 1200S vibratome in warm choline-ACSF. Slices were transferred to a standard ACSF solution containing, in mM: 127 NaCl, 2.5 KCl, 1.25 NaH₂PO₄, 25 NaHCO₃, 25 glucose, 1.5 CaCl₂, and 1 MgCl₂ maintained at 34–35 °C for

10–12 min and then stored at room temperature for at least 20 min before beginning recordings.

Whole-cell recordings of PCs were obtained with borosilicate glass electrodes of 1–2 M Ω resistance. All recordings were done at 33 °C with 2.5 μ M SR95531 (gabazine) in the bath to block inhibitory input. Visually guided recordings of PCs in Crus I were performed while holding the cell at –65 mV with an internal containing (in mM): 35 CsF, 110 CsCl, 10 Hepes, 10 EGTA, and 2 QX-314, pH adjusted to 7.2 with CsOH and osmolarity adjusted to 307 mOsm/kg. Electrophysiology data was acquired using a Multiclamp 700B amplifier (Axon Instruments), digitized at 20 kHz, and filtered at 4 kHz. For PF stimulation, theta glass electrodes filled with ACSF were placed in the molecular layer (~70 μ m apart) and applied with brief (0.5 ms) current pulse (50 μ A) for single stimulation and 20 Hz current pulses (30 μ A) for train stimulation. For single stimulation experiments, evoked response in each PC was averaged from 30 to 40 trials in 3–4 stimulating locations.

Statistical analysis

All statistical tests, significance analyses, number of individual experiments (n), and other relevant information for data comparison are specified in Supplementary Table 1. Statistical analysis was performed using commercial software (GraphPad Prism 9) and open-source Python library⁷². For all analyses, normality tests were performed first to appropriately select parametric or non-parametric methods. Significance levels are indicated as * p < 0.05, ** p < 0.01, *** p < 0.005, and not significant (ns). No statistical methods were used to predetermine sample sizes. In box plots, the bottom and top of each box are the 25th and 75th percentiles of the sample, respectively. The distance between the bottom and top of each box is the interquartile range. The bottom and top error bars indicate the most extreme values within 1.5 times the interquartile range from the 25th and 75th percentiles, respectively.

Reporting summary

Further information on research design is available in the Nature Portfolio Reporting Summary linked to this article.

Data availability

Source data supporting the figures and statistical analyses are provided with this paper. Additional datasets supporting the findings of this study are openly available in Zenodo at <https://doi.org/10.5281/zenodo.15567569>. Due to their large volume, the full raw video recordings are not publicly available but can be obtained from the corresponding author upon reasonable request. Source data are provided with this paper.

Code availability

All code used for analysis are available from the lead author upon request. The custom code used in the conditioned eyeblink and VOR analyses are available on Joon-Hyuk Lee's GitHub repository upon publication: https://github.com/ijunhyuk/publication_2025.

References

- Lee, J.-H. et al. Cerebellar granule cell signaling is indispensable for normal motor performance. *Cell Rep.* **42**, 112429 (2023).
- Wulff, P. et al. Synaptic inhibition of Purkinje cells mediates consolidation of vestibulo-cerebellar motor learning. *Nat. Neurosci.* **12**, 1042–1049 (2009).
- Peter, S. et al. AMPAR auxiliary protein shisa6 facilitates Purkinje cell synaptic excitability and procedural memory formation. *Cell Rep.* **31**, 107515 (2020).
- Kelly, E. et al. Regulation of autism-relevant behaviors by cerebellar–prefrontal cortical circuits. *Nat. Neurosci.* **23**, 1102–1110 (2020).

5. Stoodley, C. J. et al. Altered cerebellar connectivity in autism and cerebellar-mediated rescue of autism-related behaviors in mice. *Nat. Neurosci.* **20**, 1744–1751 (2017).
6. Tsai, P. T. et al. Autistic-like behaviour and cerebellar dysfunction in Purkinje cell Tsc1 mutant mice. *Nature* **488**, 647–651 (2012).
7. Hull, C. & Regehr, W. G. The cerebellar cortex. *Annu. Rev. Neurosci.* **45**, 151–175 (2022).
8. Schmahmann, J. D. The cerebellum and cognition. *Neurosci. Lett.* **688**, 62–75 (2019).
9. Chin, P. W. & Augustine, G. J. The cerebellum and anxiety. *Front. Cell. Neurosci.* **17**, 1130505 (2023).
10. Raman, I. M. & Bean, B. P. Ionic currents underlying spontaneous action potentials in isolated cerebellar Purkinje neurons. *J. Neurosci.* **19**, 1663–1674 (1999).
11. Häusser, M. & Clark, B. A. Tonic synaptic inhibition modulates neuronal output pattern and spatiotemporal synaptic integration. *Neuron* **19**, 665–678 (1997).
12. Eccles, J. C., Llinás, R. & Sasaki, K. The excitatory synaptic action of climbing fibres on the Purkinje cells of the cerebellum. *J. Physiol.* **182**, 268–296 (1966).
13. Bell, C. C. & Grimm, R. J. Discharge properties of Purkinje cells recorded on single and double microelectrodes. *J. Neurophysiol.* 1044–1055 (1969).
14. Ito, M. & Kano, M. Long-lasting depression of parallel fiber-Purkinje cell transmission induced by conjunctive stimulation of parallel fibers and climbing fibers in the cerebellar cortex. *Neurosci. Lett.* **33**, 253–258 (1982).
15. Garcia-Garcia, M. G. et al. A cerebellar granule cell-climbing fiber computation to learn to track long time intervals. *Neuron* (2024). S0896-627300366-0.
16. Wagner, M. J. et al. Cerebellar granule cells encode the expectation of reward. *Nature* **544**, 96–100 (2017).
17. Giovannucci, A. et al. Cerebellar granule cells acquire a widespread predictive feedback signal during motor learning. *Nat. Neurosci.* **20**, 727–734 (2017).
18. Broersen, R. et al. Synaptic mechanisms for associative learning in the cerebellar nuclei. *Nat. Commun.* **14**, 7459 (2023).
19. Seja, P. et al. Raising cytosolic Cl[−] in cerebellar granule cells affects their excitability and vestibulo-ocular learning. *EMBO J.* **31**, 1217–1230 (2012).
20. Galliano, E. et al. Silencing the majority of cerebellar granule cells uncovers their essential role in motor learning and consolidation. *Cell Rep.* **3**, 1239–1251 (2013).
21. Galliano, E. et al. Synaptic transmission and plasticity at inputs to murine cerebellar Purkinje cells are largely dispensable for standard nonmotor tasks. *J. Neurosci.* **33**, 12599–12618 (2013).
22. Yamamoto, M. et al. Reversible suppression of glutamatergic neurotransmission of cerebellar granule cells in vivo by genetically manipulated expression of tetanus neurotoxin light chain. *J. Neurosci.* **23**, 6759–6767 (2003).
23. Wada, N. et al. Conditioned eyeblink learning is formed and stored without cerebellar granule cell transmission. *Proc. Natl. Acad. Sci. USA* **104**, 16690–16695 (2007).
24. Wang, S. S.-H., Kloth, A. D., & Badura, A. The cerebellum, sensitive periods, and autism. *Neuron* **83**, 518–532 (2014).
25. Kim, M. et al. Regulation of cerebellar network development by granule cells and their molecules. *Front. Mol. Neurosci.* **16**, 1236015 (2023).
26. Held, R. G. et al. Synapse and active zone assembly in the absence of presynaptic Ca²⁺ channels and Ca²⁺ entry. *Neuron* **107**, 667–683.e9 (2020).
27. Aller, M. I. et al. Cerebellar granule cell Cre recombinase expression. *Genesis* **36**, 97–103 (2003).
28. Fünfschilling, U. & Reichardt, L. F. Cre-mediated recombination in rhombic lip derivatives. *Genesis* **33**, 160–169 (2002).
29. Wang, C. et al. Impaired cerebellar plasticity hypersensitizes sensory reflexes in SCN2A-associated ASD. *Neuron* **112**, 1444–1455.e5 (2024).
30. Hyde, R. J. & Rudolph, S. More than meets the eye: a conserved sensorimotor reflex helps unravel the circuit mechanisms of ASD. *Neuron* **112**, 1375–1378 (2024).
31. Parnaudeau, S. et al. Inhibition of mediodorsal thalamus disrupts thalamofrontal connectivity and cognition. *Neuron* **77**, 1151–1162 (2013).
32. Kuhlman, S. J. et al. A disinhibitory microcircuit initiates critical-period plasticity in the visual cortex. *Nature* **501**, 543–546 (2013).
33. Gremel, C. M. & Costa, R. M. Orbitofrontal and striatal circuits dynamically encode the shift between goal-directed and habitual actions. *Nat. Commun.* **4**, 2264 (2013).
34. Han, K.-S. et al. Climbing fiber synapses rapidly and transiently inhibit neighboring Purkinje cells via ephaptic coupling. *Nat. Neurosci.* **23**, 1399–1409 (2020).
35. Iskusnykh, I. Y. et al. Aging, neurodegenerative disorders, and cerebellum. *Int. J. Mol. Sci.* **25**, 1018 (2024).
36. Silva, N. T. et al. Climbing fibers provide essential instructive signals for associative learning. *Nat. Neurosci.* **27**, 940–951 (2024).
37. Rudolph, S. et al. Cerebellum-specific deletion of the GABAA receptor δ subunit leads to sex-specific disruption of behavior. *Cell Rep.* **33**, 108338 (2020).
38. Carey, M. R. et al. Presynaptic CB1 receptors regulate synaptic plasticity at cerebellar parallel fiber synapses. *J. Neurophysiol.* **105**, 958–963 (2011).
39. Albergaria, C. et al. Locomotor activity modulates associative learning in mouse cerebellum. *Nat. Neurosci.* **21**, 725–735 (2018).
40. Albergaria, C. et al. Cannabinoids modulate associative cerebellar learning via alterations in behavioral state. *eLife* **9**, e61821 (2020).
41. Wiltchko, A. B. et al. Mapping sub-second structure in mouse behavior. *Neuron* **88**, 1121–1135 (2015).
42. Markowitz, J. E. et al. The striatum organizes 3D behavior via moment-to-moment action selection. *Cell* **174**, 44–58.e17 (2018).
43. Wiltchko, A. B. et al. Revealing the structure of pharmacobehavioral space through motion sequencing. *Nat. Neurosci.* **23**, 1433–1443 (2020).
44. Yang, X. et al. Social deficits and cerebellar degeneration in Purkinje cell Scn8a knockout mice. *Front. Mol. Neurosci.* **15**, 822129 (2022).
45. Gibson, J. M. et al. Cerebellar contribution to autism-relevant behaviors in fragile X syndrome models. *Cell Rep.* **42**, (2023).
46. Kozareva, V. et al. A transcriptomic atlas of mouse cerebellar cortex comprehensively defines cell types. *Nature* **598**, 214–219 (2021).
47. Jahnsen, H. Electrophysiological characteristics of neurones in the guinea-pig deep cerebellar nuclei in vitro. *J. Physiol.* **372**, 129–147 (1986).
48. Llinás, R. & Mühlethaler, M. Electrophysiology of guinea-pig cerebellar nuclear cells in the in vitro brain stem-cerebellar preparation. *J. Physiol.* **404**, 241–258 (1988).
49. Aizenman, C. D. & Linden, D. J. Regulation of the rebound depolarization and spontaneous firing patterns of deep nuclear neurons in slices of rat cerebellum. *J. Neurophysiol.* **82**, 1697–1709 (1999).
50. Czubyayko, U. et al. Two types of neurons in the rat cerebellar nuclei as distinguished by membrane potentials and intracellular fillings. *J. Neurophysiol.* **85**, 2017–2029 (2001).
51. Carta, I. et al. Cerebellar modulation of the reward circuitry and social behavior. *Science* **363**, eaav0581 (2019).
52. Fremont, R. et al. Abnormal high-frequency burst firing of cerebellar neurons in rapid-onset Dystonia-Parkinsonism. *J. Neurosci.* **34**, 11723–11732 (2014).
53. Snell, H. D. et al. Mechanism of stress-induced attacks in an episodic neurologic disorder. *Sci. Adv.* **8**, eabh2675 (2022).
54. van der Heijden, M. E. et al. Cerebellar nuclei cells produce distinct pathogenic spike signatures in mouse models of ataxia, dystonia, and tremor. *eLife* **12**, RP91483 (2024).

55. Khan, M. M. et al. Unusually slow spike frequency adaptation in deep cerebellar nuclei neurons preserves linear transformations on the subsecond timescale. *J. Neurosci.* **42**, 7581–7593 (2022).
56. Brown, S. T. et al. Simple spike patterns and synaptic mechanisms encoding sensory and motor signals in Purkinje cells and the cerebellar nuclei. *Neuron* **112**, 1848–1861.e4 (2024).
57. Brown, S. T. & Raman, I. M. Sensorimotor integration and amplification of reflexive whisking by well-timed spiking in the cerebellar corticonuclear circuit. *Neuron* **99**, 564–575.e2 (2018).
58. Alviña, K. et al. Questioning the role of rebound firing in the cerebellum. *Nat. Neurosci.* **11**, 1256–1258 (2008).
59. van der Heijden, M. E. *Converging and Diverging Cerebellar Pathways for Motor and Social Behaviors in Mice*. (The Cerebellum, 2024).
60. Xu, Y. et al. Retinal ON bipolar cells express a new PCP2 splice variant that accelerates the light response. *J. Neurosci. J. Soc. Neurosci.* **28**, 8873–8884 (2008).
61. Belton, T. & McCrea, R. A. Role of the cerebellar flocculus region in cancellation of the VOR during passive whole body rotation. *J. Neurophysiol.* **84**, 1599–1613 (2000).
62. Peter, S. et al. Dysfunctional cerebellar Purkinje cells contribute to autism-like behaviour in Shank2-deficient mice. *Nat. Commun.* **7**, 12627 (2016).
63. Cupolillo, D. et al. Autistic-Like Traits and Cerebellar Dysfunction in Purkinje Cell PTEN Knock-Out Mice. *Neuropsychopharmacology* **41**, 1457–1466 (2016).
64. Wu, S. et al. Implications of variable synaptic weights for rate and temporal coding of cerebellar outputs. *eLife* **13**, e89095 (2024).
65. Person, A. L. & Raman, I. M. Purkinje neuron synchrony elicits time-locked spiking in the cerebellar nuclei. *Nature* **481**, 502–505 (2012).
66. Badura, A. et al. Normal cognitive and social development require posterior cerebellar activity. *eLife* **7**, e36401 (2018).
67. Heiney, S. A. et al. Precise control of movement kinematics by optogenetic inhibition of Purkinje cell activity. *J. Neurosci.* **34**, 2321–2330 (2014).
68. Mathis, A. et al. DeepLabCut: markerless pose estimation of user-defined body parts with deep learning. *Nat. Neurosci.* **21**, 1281–1289 (2018).
69. Forman, C. J. et al. Openspritzer: an open hardware pressure ejection system for reliably delivering picolitre volumes. *Sci. Rep.* **7**, 2188 (2017).
70. Pachitariu, M. et al. *Kilosort: realtime spike-sorting for extracellular electrophysiology with hundreds of channels* (2016).
71. Buccino, A. P. et al. SpikeInterface, a unified framework for spike sorting. *eLife* **9**, e61834 (2020).
72. Vallat, R. Pingouin: statistics in Python. *J. Open Source Softw.* **3**, 1026 (2018).

Acknowledgements

We thank Shreya Palwawi, Lillian Bergin, Hailey Goffin, and Juliana Preston for their assistance with the behavioral experiments. We thank Megan R. Carey for valuable feedback. This work was supported by grants from the NIH (R35NS097284 to W.G.R.), the William Randolph

Hearst Fund, and the Ellen R. and Melvin J. Gordon Center for the Cure and Treatment of Paralysis to J.-H.L., and the Lefler Center at HMS and Eva Tan Postdoc fellowship to Shuting Wu. Imaging was performed in the Neurobiology Imaging Facility at Harvard Medical School.

Author contributions

J.-H.L. and W.G.R. conceived the experiments. J.-H.L. and C.G. established the equipment and protocols for the behavioral experiments. S.W. conducted in vitro electrophysiology experiments. A.N., Z.Y., J.-H.L., and S. S. conducted behavioral experiments. J.-H.L. analyzed behavioral data. J.-H.L. conducted in vivo recording and analysis. J.-H.L. visualized all figures. J.-H.L. and W.G.R. wrote the manuscript with inputs from the authors.

Competing interests

The authors declare no competing interests.

Additional information

Supplementary information The online version contains supplementary material available at <https://doi.org/10.1038/s41467-025-61190-6>.

Correspondence and requests for materials should be addressed to Wade G. Regehr.

Peer review information *Nature Communications* thanks Meike Van der Heijden and the other anonymous reviewer(s) for their contribution to the peer review of this work. [A peer review file is available.]

Reprints and permissions information is available at <http://www.nature.com/reprints>

Publisher's note Springer Nature remains neutral with regard to jurisdictional claims in published maps and institutional affiliations.

Open Access This article is licensed under a Creative Commons Attribution-NonCommercial-NoDerivatives 4.0 International License, which permits any non-commercial use, sharing, distribution and reproduction in any medium or format, as long as you give appropriate credit to the original author(s) and the source, provide a link to the Creative Commons licence, and indicate if you modified the licensed material. You do not have permission under this licence to share adapted material derived from this article or parts of it. The images or other third party material in this article are included in the article's Creative Commons licence, unless indicated otherwise in a credit line to the material. If material is not included in the article's Creative Commons licence and your intended use is not permitted by statutory regulation or exceeds the permitted use, you will need to obtain permission directly from the copyright holder. To view a copy of this licence, visit <http://creativecommons.org/licenses/by-nc-nd/4.0/>.

© The Author(s) 2025